creative commons
COMMONS DEED

저작자표시-비영리-변경금지 2.0 대한민국

이용자는 아래의 조건을 따르는 경우에 한하여 자유롭게

- 이 저작물을 복제, 배포, 전송, 전시, 공연 및 방송할 수 있습니다.

다음과 같은 조건을 따라야 합니다:

저작자표시. 귀하는 원저작자를 표시하여야 합니다.

비영리. 귀하는 이 저작물을 영리 목적으로 이용할 수 없습니다.

변경금지. 귀하는 이 저작물을 개작, 변형 또는 가공할 수 없습니다.

- 귀하는, 이 저작물의 재이용이나 배포의 경우, 이 저작물에 적용된 이용허락조건을 명확하게 나타내어야 합니다.
- 저작권자로부터 별도의 허가를 받으면 이러한 조건들은 적용되지 않습니다.

저작권법에 따른 이용자의 권리는 위의 내용에 의하여 영향을 받지 않습니다.

이것은 이용허락규약(Legal Code)을 이해하기 쉽게 요약한 것입니다.

Disclaimer

dCollection

M.S. THESIS

A Mobile VR Motion Controller with 6 DoF positioning using Light Polarization

편광을 활용한 6 자유도 위치추적 모바일 VR 컨트롤러

FEBRUARY 2020

DEPARTMENT OF COMPUTER SCIENCE AND ENGINEERING
COLLEGE OF ENGINEERING
SEOUL NATIONAL UNIVERSITY

Hyouk JANG

M.S. THESIS

A Mobile VR Motion Controller with 6 DoF positioning using Light Polarization

편광을 활용한 6 자유도 위치추적 모바일 VR 컨트롤러

FEBRUARY 2020

DEPARTMENT OF COMPUTER SCIENCE AND ENGINEERING
COLLEGE OF ENGINEERING
SEOUL NATIONAL UNIVERSITY

Hyouk JANG

A Mobile VR Motion Controller with 6 DoF positioning using Light Polarization

편광을 활용한 6 자유도 위치추적 모바일 VR 컨트롤러

지도교수 김건희

이 논문을 공학석사학위논문으로 제출함

2019 년 11 월

서울대학교 대학원

컴퓨터공학부

장혁

장혁의 석사학위논문을 인준함

2020 년 1 월

위 원 장	장 병 탁	(인)
부위원장	김 건 희	(인)
위 원	강 유	(인)

Abstract

A Mobile VR Motion Controller with 6 DoF positioning using Light Polarization

Hyouk JANG
Department of Computer Science and Engineering
College of Engineering
Seoul National University

We introduce *POL360*: the first universal VR motion controller that leverages the principle of *light polarization*. POL360 enables a user who holds it and wears a VR headset to see their hand motion in a virtual world via its accurate 6-DOF position tracking. Compared to other techniques for VR positioning, POL360 has several advantages as follows. (1) *Mobile compatibility*: Neither additional computing resource like a PC/console nor any complicated pre-installation is required in the environment. Only necessary device is a VR headset with an IR LED module as a light source to which a thin-film linear polarizer is attached. (2) *On-device computing*: Our POL360's computation for positioning is completed on the microprocessor in the device. Thus, it does not require additional computing resource of a VR headset. (3) *Competitive accuracy and update rate*: In spite of POL360's superior mobile compatibility and affordability, POL360 attains competitive performance of accuracy and fast update rates. That is, it achieves the subcentimeter accuracy of positioning and the tracking rate higher than 60 Hz. In this paper, we derive the mathematical formulation of 6-DOF positioning using light polarization for the first time and implement a POL360 prototype that can directly operate with any commercial VR headset systems. In order to demonstrate POL360's performance and usability, we carry out thor-

ough quantitative evaluation and a user study and develop three game demos as use cases.

Keywords: Virtual reality, light polarization, spatial interaction, 3-dimensional positioning

Student Number: 2016-26445

Contents

Abstract **i**

Contents **iii**

List of Figures **v**

List of Tables **viii**

Chapter 1 Introduction **1**

Chapter 2 Related Works **4**

2.1 Computer Vision Techniques using RGB or Infrared cameras . . 4

2.2 Laser Lighthouse Tracking Techniques 5

2.3 Magnetic Sensing Techniques 6

2.4 Ultra-wideband (UWB) Techniques 6

2.5 Acoustic Sensing Techniques 7

2.6 Other Techniques 7

Chapter 3 Principles and Algorithms **9**

3.1 Background: Polarization and Malus' Law 9

3.2 Problem Formulation 10

3.3 A Sensing Module 11

3.4 Light Incidence from Intensity Measurement 12

3.5 The Reference and POL Coordinates 15
3.6 Known Parameters 16
3.7 6-DOF Positioning of POL360 17

Chapter 4 Implementation of POL360 **20**
4.1 Hardware 21
4.2 Software 21

Chapter 5 Evaluation of 6-DOF Positioning Performance **23**

Chapter 6 Example Applications **27**
6.1 A Shooting-style Demo 27
6.2 A Fruits-slicing-with-Ax Demo 28
6.3 A Whack-a-mole Demo 28
6.4 A Squash Demo 28

Chapter 7 A User Study **29**

Chapter 8 Limitations and Future Work **31**
8.1 Multiple Light Sources 31
8.2 Modeling the Shape of Light Ray 32

Chapter 9 Conclusion **33**

요약 **37**

Acknowledgements **38**

List of Figures

Figure 1.1 *POL360* is a mobile motion controller for VR applications leveraging the principle of light polarization. POL360 enables a user to see their hand motion in a virtual world via its accurate 6-DOF position tracking with no pre-installation required in the environment. POL360 works with any VR headset with an IR LED module as a light source to which a thin-film linear polarizer is attached. . 2

Figure 3.1 The light polarization. We present the intensity changes when unpolarized light passes through two linear polarizers. 9

Figure 3.2 Intuition of polarization-based position tracking. A sensing module shaped as a regular polyhedron computes its 6-DOF position by detecting the intensities of polarized light from the source in each face. 11

Figure 3.3 A *quad*: Four light sensors are deployed in each plane, and at top of the sensors, thin-film linear polarizers are attached with different polarization angles. 12

Figure 3.4 A *Dodecahedron Sensing Module* (DSM). For illustration purpose, we show only its three planes with the maximum measured intensities. In the left, we focus on a single quad in which a light intersection is shown in a quad plane. See text for the description of notation. . . 12

Figure 3.5 The geometric model for the 6-DOF POL360 positioning. We present several key parameters in POL360 and reference coordinates. See text for details. 13

Figure 3.6 Coordinate transformations. (a) T_G: Frame POL360 $\rightarrow$ Frame *G*. (b) T_{PD} : Frame $G \rightarrow$ Frame *PD* (c) T_{Ref} : Frame *reference* $\rightarrow$ Frame *PD*. 16

Figure 4.1 A POL360 prototype and its component breakdown, including a DSM with 11 Quads, an IMU sensor, a processing board and a battery. 20

Figure 4.2 Views of a quad in the left and a DSM in the right. A quad is designed as a regular pentagon, and attached to each plane of the DSM. 21

Figure 4.3 The *ARME* as an apparatus to measure the 6-DoF position accuracy between (a) the polarized light source and (b) an attached DSM of POL360. (c) α, β and γ are Euler angles of DSM (y,x and z rotation), and r is the distance between DSM and light source. 22

Figure 5.1 (a) A shooting-style game demo. A user moves POL360 to control a gun that shoots a bullet to burst the targets. (b) A fruits-slicing-with-ax demo. A user slices the fruits popped out from the barrel using an ax controlled by POL360. (c) A whack-a-mole demo. Moles are popping up from their holes at random. A user controls a hammer by POL360 to hit the moles back into their holes. (d) A squash demo. Balls come from the box to a user, who should hit the ball back using a racket controlled by POL360. 26

Figure 7.1 The score distribution of the user study about VR sickness. 20 participants assign the scores in a range of $[-10, 10]$, where a positive score indicates that a user feels less sickness when using POL360 than GearVR touchpad. The score magnitude is proportional to the strength of their preference. The average score is 7.45. 30

List of Tables

Table 5.1 Four experimental results for positional accuracy and precision performance of POL360 using the *ARME*. Each set of experiments is *large-scale* as shown in the number of evaluations points by changing α, β, γ and r by $\triangle$ one at a time in the range. We report the average of accuracy (*i.e.*the ℓ_2-norm error) and precision (*i.e.*the standard deviation). The mean positional accuracy and precision of all experiments are 0.691 and 0.73, respectively. 24

Table 5.2 The power consumption and the motion-to-photon latency of POL360. We report the required power for the light source attached to the mobile VR HMD and POL360. 25

Chapter 1

Introduction

Recently, many immersive and affordable VR headsets have appeared in the market, thanks to several significant technical advances in high density displays, 3D graphics, and orientation tracking. Some notable examples include Oculus Rift, HTC Vive [10], Samsung Gear VR, HTC Vive Focus [10] and Oculus Quest [20] to name a few. Although users are now able to see in a realistic 3D virtual world through the VR headsets, one typical complaint from users in VR applications is that they passively see the virtual world like an observer or a bystander but have few means to give any input to the world.

Towards achieving natural 3D interactions in virtual reality, one of the most demanding technologies is accurate and portable positional tracking [7]. In other words, the VR system needs to track the position of a user's hands (or an object in hands) and display their physical motion in the virtual world. Recently, multiple prototypes of 3D interaction devices are about to arrive, utilizing different techniques (*e.g.*RGB or infrared cameras, laser lighthouse tracking and magnetic/acoustic/ultra-wideband/arm-body tracking sensors), as we will thoroughly review and compare in the next section.

The key contribution of this work is to propose a universal motion con-

Figure 1.1 *POL360* is a mobile motion controller for VR applications leveraging the principle of light polarization. POL360 enables a user to see their hand motion in a virtual world via its accurate 6-DOF position tracking with no pre-installation required in the environment. POL360 works with any VR headset with an IR LED module as a light source to which a thin-film linear polarizer is attached.

troller for virtual reality that leverages the *light polarization*. There has been no previous work to exploit the light polarization for the localization of a VR motion controller. We name the proposed device as *POL360*, which stands for a ***P****osition and* ***O****rientation tracking system with* ***L****ight polarization*. We derive the mathematical formulation of the 6-DOF position tracking using light polarization along with an inertial measurement unit (IMU) (section 3). We then describe the implementation of a POL360 prototype that can directly operate with any current commercial HMD systems (section 4). We carry out several

experiments to quantitatively evaluate the positioning accuracies (section 5). We also implement four game demos by ourselves as use cases (section 6) and perform a user study to demonstrate its usability (section 7). Compared to other techniques for VR positioning, we highlight several advantages of our light polarization-based approach as follows.

- **Mobile compatibility**. As shown in Figure 1.1, POL360 is a portable device in the shape of a wand. More importantly, neither additional computing resource like a PC/console nor complicated pre-installation is required in the environment. Only necessary device is a VR headset with an IR LED module as a light source to which a thin-film linear polarizer is attached. It is compatible with any mobile VR platforms such as Google cardboards, Samsung GearVR and Pico VR.

- **On-device computing**. Our POL360's computation for positioning is completed on the microprocessor in the device. Thus, it does not rely on any computing resource of a VR headset.

- **Competitive accuracy and update rate**. Despite POL360's superior mobile compatibility, POL360 attains competitive performance of accuracy and update rate. The positional mean error and precision of POL360 are measured as about 0.691 cm and 0.73 cm respectively, as will be presented in detail in our experiments of section 5. We also observe that the tracking rate is ¿ 60 Hz (*i.e.*the latency is 16.67 ms).

Chapter 2

Related Works

We review related papers and commercial products about position tracking for VR applications. We classify the tracking technologies into five groups as follows.

2.1 Computer Vision Techniques using RGB or Infrared cameras

One popular VR positioning approach is to apply object tracking techniques to the imagery obtained from RGB or Infrared cameras. The Sony PlayStation MOVE [4] is a hand-held motion-sensing game controller, which is equipped with inertial sensors and an RGB-LED lighted sphere atop it. The PlayStation webcam Eye detects the colored sphere to track the absolute position of the MOVE controller along with help of inertial sensors. The Leap Motion [19, 30] develops a series of systems that track users' hands using infrared stereo cameras. It enables a user to see their hands via HDMs in a virtual world. The Oculus Touch [27] is a pair of VR input devices that work with Oculus Rift to deliver a hand presence in a virtual world. Its 6-DOF motion tracking is

achieved by the joint use of an IR camera and an IMU. The Oculus Quest [20] also features two VR input devices for Oculus VR headset using several cameras to track 6-DOF controller. Its 6-DOF motion tracking is based on the inside-out tracking using cameras in the VR headset. The HTC Vive Focus [10] is a similar pair of VR input devices for the HTC Vive headset that includes cameras attached in front of the headset. Its 6-DOF motion tracking is implemented using the similar inside-out tracking with the Oculus Question.

Although this approach can provide users with high-quality user experience at low cost, it often needs high computing resources to extract and track the target objects from image streams, which becomes a burden to be mobile compatible. In addition, its precision could be low, depending on the camera resolution. Finally, most products in the market are platform-dependent; for example, Oculus cameras cannot be used with SONY and HTC controllers.

2.2 Laser Lighthouse Tracking Techniques

The HTC Vive [28] is one of the most successful and leading *room-scale* tracking systems for virtual reality. It can track users' movement with high precision in about a 4.6m $\times$ 4.6m space. Its two lighthouse base stations flood non-visible light in an entire room using a grid of stationary LEDs and a pair of spinning laser emitters. The receivers installed on the VR headset and controllers detect the flashes and laser beams using photosensors, and measure the relative distances with respect to the lighthouses.

The key merit of this approach is very high precision and accuracy with a room-scale tracking support. However, it is not mobile compatible unlike POL360. It is an expensive, heavy system equipped with high-tech hardware to synchronize the timing between two lighthouses, a headset and controllers. It also needs an additional high-end PC for computation of tracking multiple devices. Finally, it may be complicated for general users to install and maintain the system in the environment, and thus the HTC Vive provides installation

service by professionals.

2.3 Magnetic Sensing Techniques

The magnetic positioning is performed by measuring the intensity of the magnetic fields that a base station generates in the form of AC, DC, or pulsed DC excitation. This technique has been adopted in multiple VR controllers [1, 22, 24]. The Sixense's Stem [24] is one of electromagnetic VR motion tracking systems available in the market. It tracks full positions and orientations of multiple devices in a precision of 3 mm and 2 degrees with less than 10 ms of latency. A full body can be tracked by installing the devices on head and all four limbs (*i.e.*wrists and ankles). AccuPS's AeroWand [1, 13] is an alternative system towards multiple point tracking, which supports both mobile and PC VR systems.

One key edge of magnetic positioning is that it avoids the occlusion problem because the magnetic field can pass through many indoor objects like the wall. However, it demands a base station to release a strong magnetic signal for acceptable accuracy. Moreover, it may suffer from a fading problem caused by the multipath effect, which may cause a low precision.

2.4 Ultra-wideband (UWB) Techniques

The *Ultra-wideband* (UWB) radio technology is originally developed for transmitting information over a short-range, high-bandwidth communication. Later the UWB has been actively applied to positioning systems, which are divided into three categories; time-of-arrival, direction-of-arrival, and signal-strength based systems [11]. The merits of UWB positioning include better localization accuracies than Wi-Fi, Bluetooth, RFID, or GPS, thanks to its high bandwidth, and penetrability for building materials to some extent [17]. The *pozyx* [16] is one of commercial systems that exploit the UWB technology for localization

and motion sensing. It consists of five modules: four fixed anchors as references (*e.g.*like the satellites in GPS) and one tag whose location is tracked. Its position accuracy is of a few centimeters with an update rate of 5–10Hz.

Although this approach enjoys a high precision in general, it requires relatively expensive equipment, including a base station to release UWB RF signal. Moreover, similarly to magnetic sensing and RF-based techniques, it also suffers from a fading problem by the multipath effect.

2.5 Acoustic Sensing Techniques

The acoustic-based methods, mainly using ultrasound, perform positioning by measuring the travel time of acoustic signals between known transmitters and receivers. Some examples of its indoor localization and tracking include [18, 23]. The acoustic-based methods can achieve high resolution and accuracy at low cost, because the speed of ultrasound (*i.e.*343 m/s) is much slower than other radio signals, which allows to measure the time of flight even at a low sampling rate. The *ellipticlabs* [15] provides ultrasonic-based user interface solutions for mobile devices, which sense hand gestures and proximity in front and on all sides of the mobile phone. The *echolocus* [8] develops a free-roam/walking VR platform where the location of a user who wears an HMD is tracked using low-cost ultrasound units.

Its major advantage is that it can achieve relatively high precision and accuracy with inexpensive equipment. However, it can suffer from the Doppler effect problem, which may cause a low linearity between movement and measurement.

2.6 Other Techniques

Finally, it is worth noting Google's *Daydream* [5], which is a mobile and portable motion controller like POL360. However, *Daydream* that is equipped with only an IMU and thus is a 3-DOF device with no location tracking, which can be a

severe limitation for its applicability in 3D positioning.

The FinchShift [26] provides 6-DOF tracking of arms and body for smartphone VR headset based on their limited movement. However, a user needs to wear specific arm-band to track the controller movement. Although it is not yet released which technique is used for the arm and body tracking, it can be implemented using the measurement of magnetic fields and IMU without any camera and laser scanner.

In computer vision and graphics, there have been several attempts to leverage the principle of polarization for estimating surface normals [2], surface reflectances [21], and diffuse and specular separation [14, 12]. However, our work is unique in applying polarization to 6-DoF positional tracking for VR applications.

Chapter 3

Principles and Algorithms

In this section, we first review some background knowledge about polarization and then present the mathematical formulation of 6-DOF positioning using the polarized light.

3.1 Background: Polarization and Malus' Law

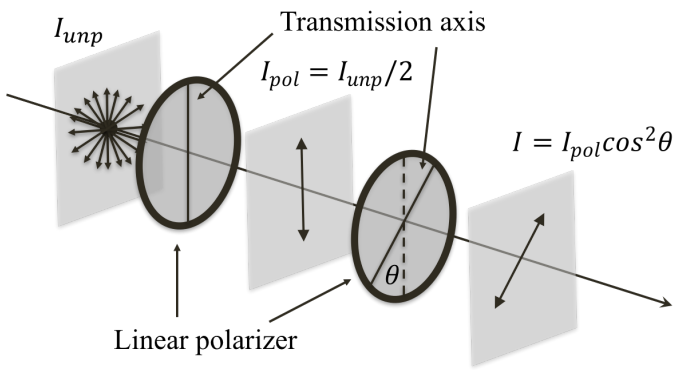

Figure 3.1 The light polarization. We present the intensity changes when unpolarized light passes through two linear polarizers.

An electromagnetic wave, including light, is a *transverse wave* in which

both an electric and a magnetic field oscillate in different directions while they maintain perpendicular to each other [9]. An ambient light is an *unpolarized* light, meaning that its electric and magnetic vibrations occur in multiple planes. A *polarizer* is an optical filter that passes only the light of a specific polarization and blocks waves of other polarizations. For example, a linear polarizer has its own plane of polarization, and passes only the component of a polarized light vector aligned by it. Figure 3.1 illustrates the polarization of the ambient light incidence to a pair of linear polarizers. We remind the two important equations about polarization as follows.

$$I_{POL} = I_{unp}/2, \tag{3.1}$$

$$I_{fin} = I_{POL} \cos^2 \theta. \tag{3.2}$$

A linear polarizer blocks a half of the incident ambient (unpolarized) light as in Equation (3.1), causing the electric field component to displace so that it oscillates in only one plane with respect to the direction of propagation. When the polarized light passes through another polarizer, the intensity of the light is described by Equation (3.2), which is known as *Malus' law*, where I_{POL} is the intensity of incident light, and θ is the angle between the light's initial polarization direction and the transmission axis of the next polarizer.

Localization using polarization is also observed in nature; for example, it is well known that bees and ants reply on polarized skylight to find out their homeward courses, whenever the main compass cue, the sun, is obscured by clouds [29].

3.2 Problem Formulation

As shown in Figure 3.2, our system consists of a light source and a sensing module whose pose and location are tracked. We place a thin-film linear polarizer in front of the light source. Thus, all the light from the source is plane-polarized

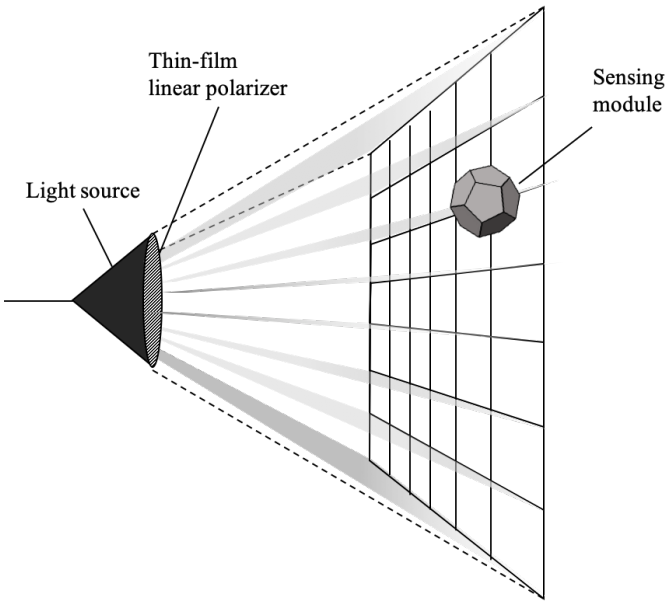

Figure 3.2 Intuition of polarization-based position tracking. A sensing module shaped as a regular polyhedron computes its 6-DOF position by detecting the intensities of polarized light from the source in each face.

at a particular angle (denoted by a unit vector $\overrightarrow{\mathbf{PD}}_{light}$ in the model later). We make a sensing module shaped as a regular polyhedron in which each face has different surface normal. We measure the light intensity detected in each face, from which we obtain the 6-DOF pose of the sensing unit using Malus'law.

3.3 A Sensing Module

We first define a planar sensing unit called a *quad* shown in Figure 3.3. The quad is attached to each face of the polyhedron sensing unit. On a plane, we deploy four light sensors, on top of which four thin-film linear polarizers are placed with different transmission axis: $\{0, \pi/4, \pi/2, 3\pi/4\}$.

We design the sensing unit, a part of which is shown in Figure 3.4, to be a regular polyhedron, all of whose faces are equipped with *quads* and have different surface normals that satisfy the linear independence condition one

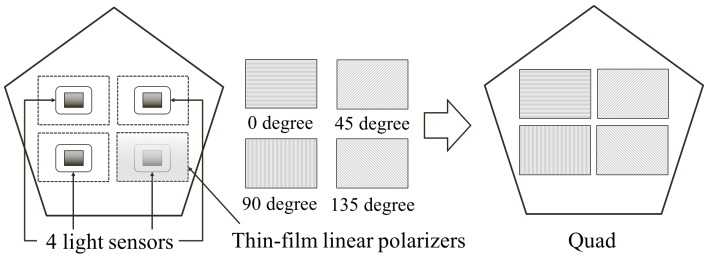

Figure 3.3 A *quad*: Four light sensors are deployed in each plane, and at top of the sensors, thin-film linear polarizers are attached with different polarization angles.

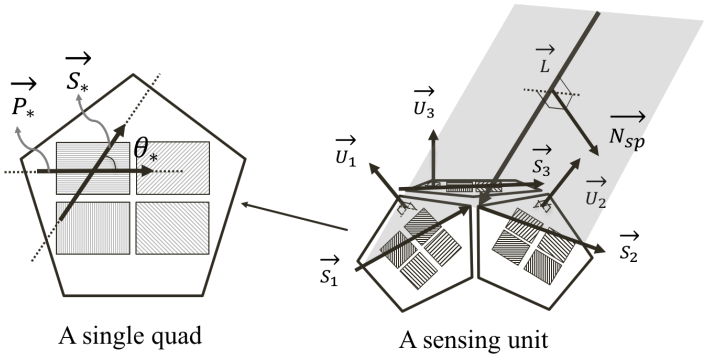

Figure 3.4 A *Dodecahedron Sensing Module* (DSM). For illustration purpose, we show only its three planes with the maximum measured intensities. In the left, we focus on a single quad in which a light intersection is shown in a quad plane. See text for the description of notation.

another. We implement the sensing unit as a dodecahedron, because it is easily manufacturable and guaranteed that at least three faces are stably illuminated from any direction of a light source. We name the sensing unit as *Dodecahedron Sensing Module* (DSM).

3.4 Light Incidence from Intensity Measurement

We describe the mathematical model to compute the light incidence direction from intensity measurement of the DSM.

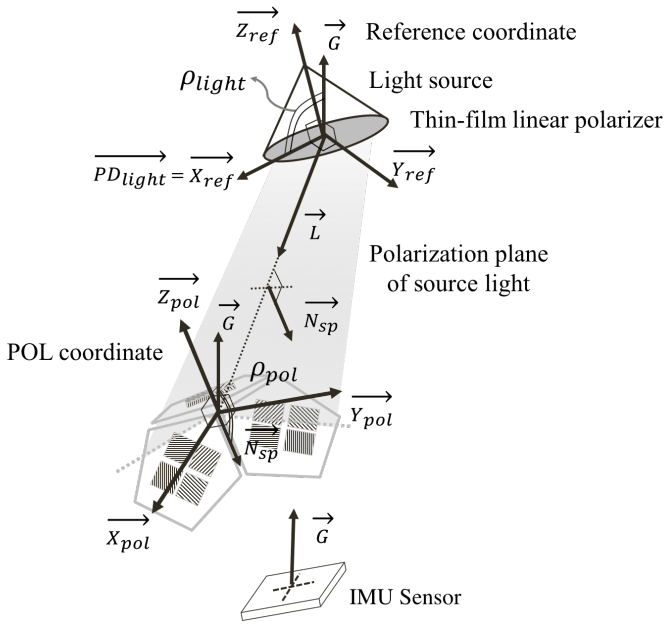

Figure 3.5 The geometric model for the 6-DOF POL360 positioning. We present several key parameters in POL360 and reference coordinates. See text for details.

Let us first focus on a single quad. We use D_x to denote the light intensity measured by a light sensor under the polarizer with a transmission angle of x: We can represent D_x as follows.

$$D_x = I_p \cos^2(\theta - x) + I_{np}/2 \quad \text{where } x = \{0, \frac{\pi}{4}, \frac{\pi}{2}, \frac{3\pi}{4}\}, \tag{3.3}$$

where I_p is the intensity of the linearly polarized source light, and I_{np} is the intensity of uncontrolled (unpolarized) ambient light from environment. In Equation (3.3), the first term is obtained by Malus' law of Equation (3.2), and the second term comes from Equation (3.1) that the light sensor measures ambient unpolarized light that passes through the linear polarizer on top of it (*i.e.*division by 2). Figure 3.4 better visualizes θ, which is the angle between $\vec{\mathbf{P}}$ and $\vec{\mathbf{S}}$, where $\vec{\mathbf{P}}$ is the unit directional vector of the base polarizer with the 0° transmission axis, and $\vec{\mathbf{S}}$ is the unit vector that indicates the line of intersection in a quad plane by the slice plane of polarized source light.

From the four equations of (3.3), we can cancel out the second term of ambient light as follows:

$$\begin{aligned} D_0 - D_{\pi/2} &= I_p \cos^2(\theta) - I_p \cos^2(\theta - \pi/2) \\ &= I_p(\cos^2(\theta) - \sin^2(\theta)) = I_p \cos(2\theta), \qquad (3.4) \\ D_{\pi/4} - D_{3\pi/4} &= I_p \cos^2(\theta - \pi/4) - I_p \cos^2(\theta - 3\pi/4) \\ &= I_p(\cos^2(\theta - \pi/4) - \sin^2(\theta - \pi/4)) \\ &= I_p \cos(2\theta - \pi/2) = I_p \sin(2\theta). \qquad (3.5) \end{aligned}$$

From Equation (3.4)–(3.5), we then represent θ and I_p as follows:

$$\theta = \frac{1}{2} \arctan(D_{\pi/4} - D_{3\pi/4}/D_0 - D_{\pi/2}), \qquad (3.6)$$

$$I_p = \sqrt{(D_0 - D_{\pi/2})^2 + (D_{\pi/4} - D_{3\pi/4})^2}. \qquad (3.7)$$

Thanks to the dodecahedron shape of the DSM, we can always find the three planes that detect the light with the maximum intensity, as shown in Figure 3.4. We denote the incident angle of light source by a unit vector $\vec{\mathbf{L}} = (L_x, L_y, L_z)$, and the surface normals of three faces by $\vec{\mathbf{U}}_{1,2,3} = (U_{*x}, U_{*y}, U_{*z})$. The intensity of each plane is proportional to the cosine of the angle between the light incidence and the surface normal: $I_{pi} \propto \vec{\mathbf{U}}_i \cdot \vec{\mathbf{L}}$. Therefore, the measured intensity in the three planes are

$$\begin{bmatrix} I_{p1} \\ I_{p2} \\ I_{p3} \end{bmatrix} = \kappa \begin{bmatrix} U_{1x} & U_{1y} & U_{1z} \\ U_{2x} & U_{2y} & U_{2z} \\ U_{3x} & U_{3y} & U_{3z} \end{bmatrix} \begin{bmatrix} L_x \\ L_y \\ L_z \end{bmatrix}. \qquad (3.8)$$

where κ is a constant. Since we measure I_{p1}, I_{p2}, I_{p3} and know $\vec{\mathbf{U}}_{1,2,3}$ from the DSM geometry, we can compute $\vec{\mathbf{L}}$ by solving Equation (3.8) along with the constraint $\|\vec{\mathbf{L}}\| = 1$.

3.5 The Reference and POL Coordinates

Figure 3.5 illustrates our geometric model to compute the pose of POL360. We first define two coordinates named *reference coordinates* and *POL coordinates*.

The origin of the reference coordinates is set at the center of light source. We define $\vec{\mathbf{Z}}_{ref}$ as the opposite to the light direction, and $\vec{\mathbf{X}}_{ref}$ as the transmission axis of the linear polarizer attached to the light source. Finally, $\vec{\mathbf{Y}}_{ref}$ is uniquely defined by a cross product $\vec{\mathbf{Y}}_{ref} = \vec{\mathbf{Z}}_{ref} \times \vec{\mathbf{X}}_{ref}$. Based on this definition, the polarization plane of the source light is represented by $\vec{\mathbf{y}}_{ref} = c$, where c is any constant.

The origin of the POL coordinates is defined at the intersection of the three planes with the maximum incident light. We define $\vec{\mathbf{Z}}_{POL}$ as the upward direction of POL360. We then let $\vec{\mathbf{X}}_{POL}$ to be the direction to the button which is attached POL360. (See the Figure 4.1). Finally, $\vec{\mathbf{Y}}_{POL}$ is set by a cross product $\vec{\mathbf{Y}}_{POL} = \vec{\mathbf{Z}}_{POL} \times \vec{\mathbf{X}}_{POL}$. That is, the POL360 frame is fixed to POL360. Strictly speaking, it may be better to set the origin of POL360 frame at the center of the DSM, since the three planes with the maximum light incidence can be changed during the operation. However, we set the origin at the vertex of the dodecahedron for illustration easiness. It does not hurt the following formulation of the position tracking, because we exactly know the relative position of each vertex with respect to the center of the DSM, from the geometry of a POL360 prototype.

We now define additional notation depicted in Figure 3.5. Since POL360 is equipped with an IMU sensor, we can always measure the direction of gravity. We use $\vec{\mathbf{G}}$ to denote the opposite direction of gravity. We denote the angle between $\vec{\mathbf{G}}$ and $\vec{\mathbf{X}}_{ref}$ by ρ_{light}. Among the planes of polarization of the source light $\vec{\mathbf{y}}_{ref} = c$ where $c \in \mathbb{R}$, we can uniquely find the one that contains the origin of POL coordinates. We use $\vec{\mathbf{N}}_{sp}$ to denote a surface normal of the polarization plane. Note $\vec{\mathbf{N}}_{sp}$ is perpendicular to $\overrightarrow{\mathbf{PD}}_{light}$, since $\overrightarrow{\mathbf{PD}}_{light} = \vec{\mathbf{X}}_{ref}$ is parallel

to $\vec{\mathbf{y}}_{ref} = c$. We denote the angle between $\vec{\mathbf{G}}$ and $\vec{\mathbf{N}}_{sp}$ by ρ_{POL}. Finally, we represent the angle between $\vec{\mathbf{G}}$ and $\vec{\mathbf{X}}_{ref}$ by ρ_{light}.

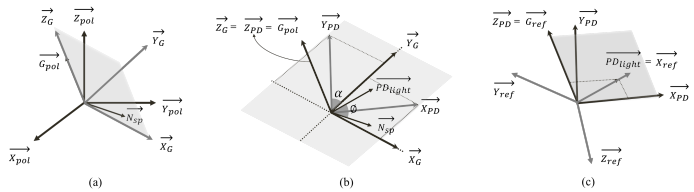

Figure 3.6 Coordinate transformations. (a) T_G: Frame POL360 $\rightarrow$ Frame G. (b) T_{PD} : Frame $G \rightarrow$ Frame PD (c) T_{Ref} : Frame *reference* $\rightarrow$ Frame PD.

3.6 Known Parameters

Among the variables described, we know the following ones with respect to POL coordinates using POL360 geometry. First, we know the surface normal $\vec{\mathbf{U}}_{1,2,3}$ and the direction of base polarizer $\vec{\mathbf{P}}_{1,2,3}$ of each quad as shown in Figure 3.4. Since we measure $\theta_{1,2,3}$ from Equation (3.6), we can obtain $\vec{\mathbf{S}}_{1,2,3}$ by rotating $\vec{\mathbf{P}}_{1,2,3}$ by $\theta_{1,2,3}$ along the axis of surface normals $\vec{\mathbf{U}}_{1,2,3}$. We also compute $\vec{\mathbf{L}}$ from measured $I_{p1,2,3}$ using Equation (3.8). The gravity direction $\vec{\mathbf{G}}_{POL}$ in the POL360 frame is also available from the IMU sensor. From Figure 3.4, we also know that the surface normal of the polarization plane $\vec{\mathbf{N}}_{sp}$, because the polarization plane contains both $\vec{\mathbf{S}}_{P1}$ and $\times\vec{\mathbf{S}}_{P2}$: That is, $\vec{\mathbf{N}}_{sp} = \vec{\mathbf{S}}_{P1} \times \vec{\mathbf{S}}_{P2}$. Finally, we can compute the angle $\rho_{POL} = \vec{\mathbf{G}}_{POL} \cdot \vec{\mathbf{N}}_{sp}$.

We also assume that we know the gravity direction $\vec{\mathbf{G}}_{ref}$ with respect to the reference frame. One simple way to know it is to use an IMU in a VR headset; for example, we can exploit a free surface level app that can be installed in a VR headset so that the light ramp directly points to the gravity direction ($i.e. \vec{\mathbf{Z}}_{ref} = \vec{\mathbf{G}}_{ref}$). Another possibility is to install an IMU to the light source. As a future development, we also consider attaching a light source to the HMD; in such case, we can read from the IMU of the HMD for $\vec{\mathbf{G}}_{ref}$. In our experiments, we test the positioning performance of POL360 using a surface level app, and

validate this approach is sufficiently accurate in practice. Finally, we obtain the angle $\rho_{light} = \vec{\mathbf{G}}_{ref} \cdot \vec{\mathbf{X}}_{ref}$.

3.7 6-DOF Positioning of POL360

We derive the 6-DOF positioning of POL360 denoted by $\boldsymbol{\chi}_{POL,ref} \in \mathbb{R}^6$ with respect to the reference coordinates. Since the POL coordinates are fixed to POL360, the positioning reduces to represent POL coordinates with respect to the reference frame. We decompose the overall transformation into three processes for easier derivation and better understanding.

(1) T_1 **: Frame POL360** $\rightarrow$ **Frame** $\boldsymbol{G}$. We define the Frame G that has $\vec{\mathbf{G}}_{POL}$ as its z-axis and $\vec{\mathbf{G}}_{POL} \times \vec{\mathbf{N}}_{sp}$ and its y-axis. We remind that $\vec{\mathbf{G}}_{POL}$ is the unit vector that the IMU sensor measures as the opposite direction of gravity in the POL coordinate. $\vec{\mathbf{N}}_{sp}$ is the normal vector of the plane of polarization of the light source. Figure 3.6.(a) illustrates the transformation from Frame POL360 to Frame G, whose basis vectors are as follows.

$$\vec{\mathbf{X}}_G = \vec{\mathbf{Y}}_G \times \vec{\mathbf{Z}}_G, \;\; \vec{\mathbf{Y}}_G = \vec{\mathbf{G}}_{POL} \times \vec{\mathbf{N}}_{sp}, \;\; \vec{\mathbf{Z}}_G = \vec{\mathbf{G}}_{POL}. \tag{3.9}$$

The 3×3 transformation matrix is $\mathbf{T}_1 = [\vec{\mathbf{X}}_G \; \vec{\mathbf{Y}}_G \; \vec{\mathbf{Z}}_G]^T$, which can be computed from known $\vec{\mathbf{G}}_{POL}$ and $\vec{\mathbf{N}}_{sp}$.

(2) T_2 **: Frame** $\boldsymbol{G}$ $\rightarrow$ **Frame** $\boldsymbol{PD}$. As shown in Figure 3.6.(b), the Frame PD shares the same z-axis with the Frame G. It is defined by rotating the Frame G along the z-axis by α so that the angle between $\vec{\mathbf{N}}_{sp}$ and $\overrightarrow{\mathbf{PD}}_{light}$ is $\phi = 90°$. We remind that ρ_{POL} is the angle between $\vec{\mathbf{G}}$ and $\vec{\mathbf{N}}_{sp}$, and ρ_{light} is the angle between $\vec{\mathbf{G}}$ and $\overrightarrow{\mathbf{PD}}_{light}$. We represent $\overrightarrow{\mathbf{PD}}_{light}$ and $\vec{\mathbf{N}}_{sp}$ as

$$\overrightarrow{\mathbf{PD}}_{light} = (\cos\rho_{light}, \sin\rho_{light}, 0), \tag{3.10}$$

$$\vec{\mathbf{N}}_{sp} = (\cos\rho_{POL}, \sin\rho_{POL}\cos\alpha, \sin\rho_{POL}\sin\alpha). \tag{3.11}$$

From $\overrightarrow{\mathbf{PD}}_{light} \cdot \vec{\mathbf{N}}_{sp} = \cos\phi = \cos 90° = 0$, we compute α as

$$\cos\alpha = \frac{\cos\phi - \cos\rho_{light}\cos\rho_{POL}}{\sin\rho_{light}\sin\rho_{POL}}. \tag{3.12}$$

Since ρ_{POL} and ρ_{light} are known, we can compute α ($i.e.$the rotation angle along the z-axis so that $\vec{\mathbf{N}}_{sp}$ is perpendicular to $\overrightarrow{\mathbf{PD}}_{light}$) from Equation (3.12). Finally, the rotation matrix is

$$\mathbf{T}_2 = \begin{bmatrix} \cos\alpha & -\sin\alpha & 0 \\ \sin\alpha & \cos\alpha & 0 \\ 0 & 0 & 1 \end{bmatrix}. \tag{3.13}$$

T_3 **: Frame *Ref* $\rightarrow$ Frame *PD***. Figure 3.6.(c) shows the transformation from Frame *Ref* to Frame *PD*. $\vec{\mathbf{G}}_{ref}$ denotes the opposite direction of gravity in the reference coordinates, and $\overrightarrow{\mathbf{PD}}_{light}$ is polarization angle of the thin-film linear polarizer attached to the light source. By definition, it is identical to $\vec{\mathbf{X}}_{ref}$. The three basis vectors of the Frame *PD* are represented by the parameters in the reference frame ($i.e.\vec{\mathbf{G}}_{ref}$, $\overrightarrow{\mathbf{PD}}_{light} = \vec{\mathbf{X}}_{ref}$):

$$\overrightarrow{\mathbf{X}}_{PD} = \vec{\mathbf{Y}}_{PD} \times \vec{\mathbf{Z}}_{PD},\ \vec{\mathbf{Y}}_{PD} = \vec{\mathbf{G}}_{ref} \times \vec{\mathbf{PD}}_{light},\ \vec{\mathbf{Z}}_{PD} = \vec{\mathbf{G}}_{ref}. \tag{3.14}$$

Therefore, the transformation matrix is $\mathbf{T}_3 = [\vec{\mathbf{X}}_{PD}\ \vec{\mathbf{Y}}_{PD}\ \vec{\mathbf{Z}}_{PD}]^T$.

Through the three processes, the transformation from the POL360 frame to the reference frame is represented by

$$\mathbf{T} = {\mathbf{T}_3}^{-1}\mathbf{T}_2\mathbf{T}_1, \tag{3.15}$$

where $\mathbf{T}_3$ is inverted because it is a transformation from Frame *Ref* to Frame *PD*. Since the rotational pose of POL360 corresponds to describing POL360 frame with respect to the reference frame, it comes to computing $\mathbf{T}$ in Equation (3.15).

We now discuss how to compute the translational position of POL360 ($i.e.$localization of the origin of POL360 frame in the reference frame). Since $\vec{\mathbf{L}}$ in Equation (3.8) is the directional vector from POL360 frame to the reference frame, $-\mathbf{T}\vec{\mathbf{L}}$ is a unit directional vector from the origin of the reference frame to that of POL360 frame. Therefore, we summarize the 6-DOF positioning of POL360 with respect

to the reference is

$$\boldsymbol{\chi}_{POL,ref} = \begin{bmatrix} f(I_p)\mathbf{T}\vec{\mathbf{L}} \\ \mathbf{T} \end{bmatrix} \text{ where} f(I_p) = -\sqrt{\frac{I_o}{I_p}}. \tag{3.16}$$

The equation for $f(I_p)$ is derived from the inverse-square law that the intensity is inversely proportional to the square of the distance from the source. I_o is a parameter to calibrate, indicating the light intensity measured at fixed position from the light source (*e.g.*10cm from the source in our experiments). However, in practice it is more important to track the incremental motion change of POL360, and thus this calibration process is not critical for its actual use.

Chapter 4

Implementation of POL360

Figure 4.1 illustrates a POL360 prototype, which is designed in the shape of a wand to provide a better grip and interaction comfort. The DSM is installed at top of the wand to minimize the occlusion of light incidence by a user's body parts. The detailed implementation of the DSM is depicted in Figure 4.2. The POL360 takes care of sensor reading, computation of algorithm and the wireless transmission of positional results to a VR headset.

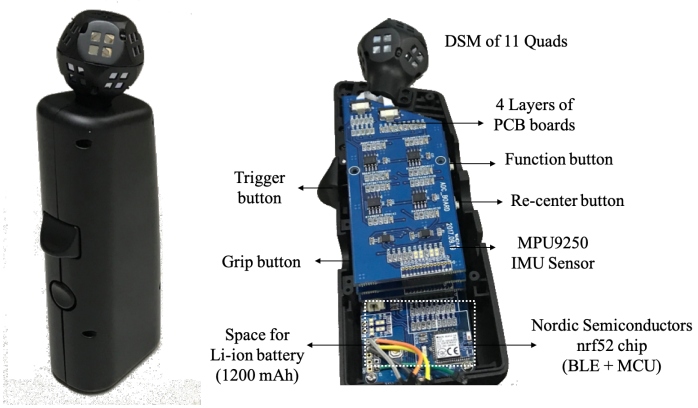

Figure 4.1 A POL360 prototype and its component breakdown, including a DSM with 11 Quads, an IMU sensor, a processing board and a battery.

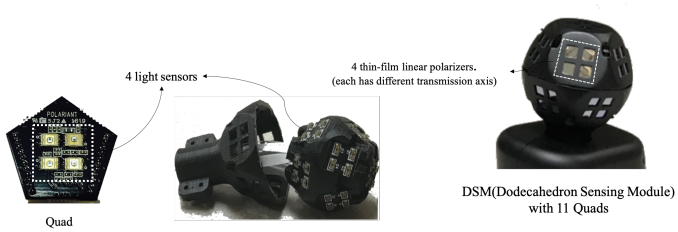

Figure 4.2 Views of a quad in the left and a DSM in the right. A quad is designed as a regular pentagon, and attached to each plane of the DSM.

4.1 Hardware

For an IMU sensor, we use MPU9250. In our first prototype, however, we only use the IMU sensor to recognize orientation and acceleration. As a sensor processing module, we use a customized PCB board, which includes NRF52 chip (BLE + MCU) of Nordic Semiconductors. Its main role is to calculate and transmit sensor reading to the a VR headset wirelessly. We use a 1200mAh Li-ion battery that provides 4 hours of active operation with stable performance.

4.2 Software

We implement the aforementioned algorithm of 6-DOF positioning in the MCU on the PCB board. The processor of POL360 internally selects the top three quads with the maximum measured intensities out of eleven quads. Then it streams raw sensor data to the MCU, including light intensity measurement from 12 light sensors in the selected three quads and the orientation information from the IMU, via Bluetooth at 115,200 baud rates. We adopt filtering to smooth raw data. In our implementation, the overall motion-to-photon tracking rate is ¿ 60 Hz (*i.e.*the latency is about 16.67 ms).

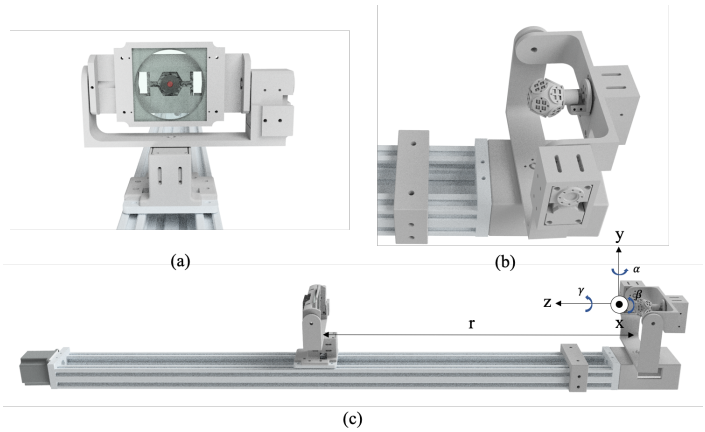

Figure 4.3 The *ARME* as an apparatus to measure the 6-DoF position accuracy between (a) the polarized light source and (b) an attached DSM of POL360. (c) α, β and γ are Euler angles of DSM (y,x and z rotation), and r is the distance between DSM and light source.

Chapter 5

Evaluation of 6-DOF Positioning Performance

We conduct experiments to evaluate the positioning performance of POL360. For the precise measurement of performance, we manufacture an experimental equipment named *ARME* (Automated Rotational Matrix Equipment) in Figure 4.3. The *ARME* is an apparatus that controls the 6-DOF relative positions of the sensing module DSM of POL360 with respect to a fixed polarized light source. We denote the three Euler angles of the DSM as α, β and γ and the distance from the light source to the DSM as r.

Table 5.1 shows the results of positional accuracy and precision from four different sets of experiments using the ARME. In each experiment, we set the range of α, β, γ and r with a resolution of $\triangle$. The ranges of Euler angles are determined based on the working range in usual VR applications; for example, the range of γ is larger than those of α and β since it reflects the left and right movement of wrists. While changing each parameter by $\triangle$ one at a time, we compute the accuracy metric as the ℓ_2 difference between the actual coordinates and the estimated ones by POL360. The precision is a description of random errors; we calculate the empirical standard deviation, which is a useful and com-

Table 5.1 Four experimental results for positional accuracy and precision performance of POL360 using the *ARME*. Each set of experiments is *large-scale* as shown in the number of evaluations points by changing α, β, γ and r by $\triangle$ one at a time in the range. We report the average of accuracy (*i.e.*the ℓ_2-norm error) and precision (*i.e.*the standard deviation). The mean positional accuracy and precision of all experiments are 0.691 and 0.73, respectively.

No	α(rad)			β(rad)			γ(rad)			r(cm)			# evaluation	accuracy	precision
	start	end	$\triangle$	start	end	$\triangle$	start	end	$\triangle$	start	end	$\triangle$	points	(cm)	(σ, cm)
1	$-\pi/9$	$\pi/9$	$\pi/36$	$-\pi/9$	$\pi/9$	$\pi/36$	$-\pi/2$	$\pi/2$	$\pi/6$	20	60	3	7938 (9×9×7×14)	0.774	0.832
2	$-\pi/9$	$\pi/9$	$\pi/36$	$-\pi/9$	$\pi/9$	$\pi/36$	$-\pi/2$	$\pi/2$	$\pi/6$	20	61	0.5	47061 (9×9×7×83)	0.795	0.812
3	$-\pi/12$	$\pi/12$	$\pi/36$	$-\pi/12$	$\pi/12$	$\pi/36$	$-\pi/2$	$\pi/2$	$\pi/8$	20	80	60	882 (7×7×9×2)	0.641	0.623
4	$-\pi/18$	$\pi/18$	$\pi/36$	$-\pi/18$	$\pi/18$	$\pi/36$	$-\pi/2$	$\pi/2$	$\pi/8$	20	80	5	2925 (5×5×9×13)	0.552	0.653

monly used measure of precision. The mean positional accuracy and precision of POL360 for all experiments in Table 5.1 are **0.691** and **0.73**, respectively. We observe that the accuracy in Experiment 4 is the best as its range of α and β are the lowest. In all experiments, the positioning error is far less than 1 cm, which validates that POL360 is sufficiently accurate as a commercial product.

It is not easy to directly compare the accuracy performance of POL360 with those of existing papers and commercial systems, because there are no previous work for VR motion controllers that are comparable to POL360 and commercial systems often do not release these statistics in public. Borrego *et al.*[3] empirically measure the accuracy of Oculus Rift and HTC Vive for rehabilitation purpose and respectively report their accuracies at standing position (1.7 m of height) by about **0.61**$\pm$0.55 cm **1.22**$\pm$1.18 cm inside the working area that the manufactures recommend. The mean positional accuracy of POL360 is **0.691** cm, which implicates that POL360 is comparable to other commercial systems in terms of 3D positioning performance[1].

Table 5.2 summarizes the power consumption of POL360 and the light source attached to the mobile HMD. We also measure the *motion-to-photon* latency, which is the time needed to fully reflect a user movement on a display screen. Our latency of 16.67 ms corresponds to a refresh rate of about 60 Hz; therefore, a user may not feel any delay from the controller. Again, it is hard to

[1]A disclaimer here is that the experimental settings between ours and [3] are different. Therefore, the numbers are comparable not exactly but roughly.

Table 5.2 The power consumption and the motion-to-photon latency of POL360. We report the required power for the light source attached to the mobile VR HMD and POL360.

Power comsuption(W)				Latency(ms)
light source	POL360			
	active	idle	sleep	
0.97	0.30	0.28	0.28	16.67

exactly compare the power consumption and the latency with other commercial systems due to lack of reported numbers. Nonetheless, we can easily expect these specifications of POL360 are sufficiently good as a commercial product. The power consumption of POL360 is much lower than that of any VR headset, which means that the running time of POL360 is much longer than that of the headset. The refresh rate of POL360 is also enough for most VR applications since most commercial controllers target at 50–60 Hz and a user usually feel no difference of latency if higher than 60 Hz.

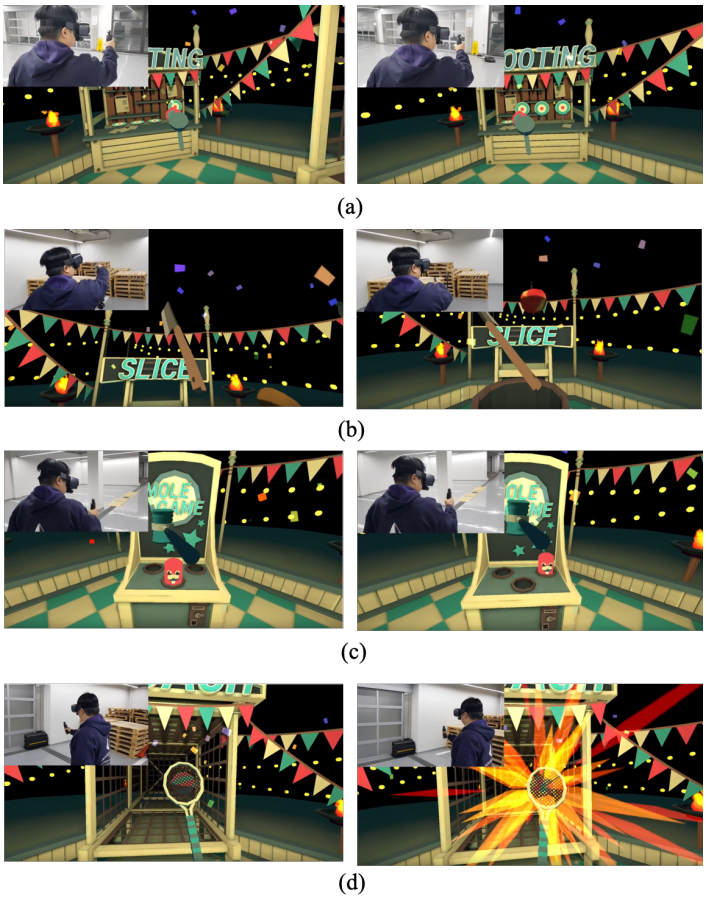

Figure 5.1 (a) A shooting-style game demo. A user moves POL360 to control a gun that shoots a bullet to burst the targets. (b) A fruits-slicing-with-ax demo. A user slices the fruits popped out from the barrel using an ax controlled by POL360. (c) A whack-a-mole demo. Moles are popping up from their holes at random. A user controls a hammer by POL360 to hit the moles back into their holes. (d) A squash demo. Balls come from the box to a user, who should hit the ball back using a racket controlled by POL360.

Chapter 6

Example Applications

To demonstrate the usefulness of our prototype further, we develop four game demos with Unity3D by ourselves. They include a shooting-style game, a fruits-slicing game, a whack-a-mole game and a squash game in virtual reality. Those games are developed as different one another as possible to demonstrate that POL360 supports a wide range of interaction types. Enabled by POL360's mobile compatible features, a user can portably play VR games. The supplementary video details how to play the games.

6.1 A Shooting-style Demo

The first demo is a shooting-style game in Figure 5.1(a). A user moves POL360 to control the position and orientation of the stick gun in a 3D virtual world. The goal of the game is to burst the targets in front of users by pressing the button, which shoots bullets. Figure 5.1 shows pairs of actual playshots and screenshots that a user sees via HMD. This demo shows that POL360 is an immersive controller in an arcade-style mobile VR game.

6.2 A Fruits-slicing-with-Ax Demo

Figure 5.1(b) shows a fruits-slicing-with-ax game, where a user controls an ax by POL360 to slice the fruits which are popped out from the barrel. This demo validates both POL360's fine resolution of position control and fast response time. It also shows that POL360 successfully supports interactivity in an action-style VR game.

6.3 A Whack-a-mole Demo

Figure 5.1(c) shows a demo, in which a user hits the moles from holes. When the hammer hit a mole, a user can feel the contact as a reaction. It demonstrates POL360's low latency for fast back and forth movement in virtual reality.

6.4 A Squash Demo

Figure 5.1(d) shows a squash demo where a user controls a squash racket by POL360. When the racket hits the ball, the ball bounces back into the box. It demonstrates that POL360 enables the control of a racket to send a ball in various heading directions.

Chapter 7

A User Study

We perform a simple user study to evaluate how users comfortably use POL360 as a VR controller. Since the motion sickness is one of the most common and critical side effects in VR applications, we compare between how much users experience the VR sickness when using POL360 with the built-in interface of a VR headset, for which we use a Samsung GearVR.

We recruit 20 participants who have no experience in mobile virtual reality. Most of them are software engineers, who are aged between 26 and 45 (mean= 29.3, std= 3.4) and comprised of 15 men and 5 women. We let them play the first shooting-style game in Figure 5.1 (a) for five minutes in each of two different sessions as follows. In the first session, users control the stick gun by the IMU of the VR headset. That is, users need to move their heads to see the target and press and release a touchpad on the GearVR to shoot a ball. In the second session, users use POL360 to control and shoot the stick gun.

After completing the two sessions, we obtain responses from users about which session they feel VR sickness more severely. Each user assigns a score in a range of $[-10, 10]$, where a positive (negative) score means that they feel more sickness when using the GearVR interface (POL360). The magnitude indicates

the strength of their preference, and a zero score means that they equally feel the sickness in both sessions.

Fig. 7.1 summarizes the score distributions assigned by 20 users. POL360 is unanimously favored by users with significant margins; the average score is 7.45. This result indicates that a portable VR controller is required to reduce the VR sickness and our POL360 successfully satisfies this objective.

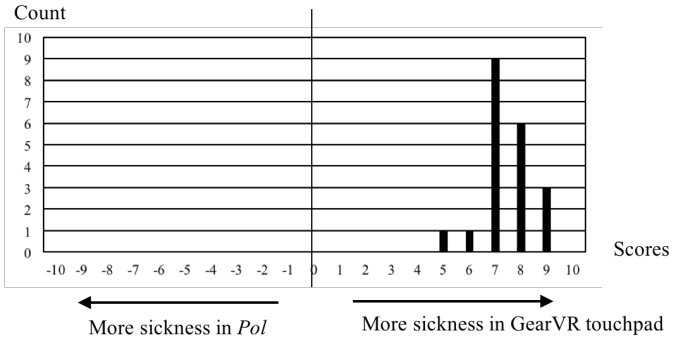

Figure 7.1 The score distribution of the user study about VR sickness. 20 participants assign the scores in a range of $[-10, 10]$, where a positive score indicates that a user feels less sickness when using POL360 than GearVR touchpad. The score magnitude is proportional to the strength of their preference. The average score is 7.45.

Chapter 8

Limitations and Future Work

POL360 achieves a precise 3D position tracking of user motion in mobile VR environment. Our experiments and demonstrations successfully show a strong potential to offer a variety of interactions. Nevertheless, the current prototype has some limitations to be explored as future work. We discuss them in two respects as follows.

8.1 Multiple Light Sources

Our formulation assumes that there is only a single light source in the environment. If POL360 operates far from the light source, the tracking can be less accurate. Using multiple light sources can alleviate the inhomogeneity of light intensity in the environment. Furthermore, more accurate positioning can be achieved using the Triangulation [6]; we obtain multiple position estimations from different light sources and compute the final pose using their weighted average. This approach is also more robust against various factors such as bias from different sensor characteristics or noise from unexpected external causes.

8.2 Modeling the Shape of Light Ray

Another limitation of the current formulation is that we do not take the shape of light ray into consideration. For example, the inverse-square law that we adopt in our model can be used only in cases where the light source approximates a point source [25]. In practice, the light ray has different shapes according to lamp types, shapes and other specification. Hence, they need to be correctly modeled to describe an accurate relation between a measured intensity and a distance from the light source. In this vein, an interesting future work of ours is to investigate a more realistic light intensity-distance model, which can lead more precise positioning.

Chapter 9

Conclusion

We introduced *POL360* as the first motion controller that leverages the light polarization for mobile VR devices. The POL360 enabled a user to see their hand motion in a virtual world via its accurate 6-DOF position tracking. Compared to other techniques for VR positioning, POL360 bears several important advantages, including mobile compatibility, affordability, and comparative accuracy and update rate. We derived the mathematical formulation of 6-DOF positioning of POL360, and described the implementation of its first prototype. We demonstrated its superior performance and usability by carrying out quantitative experiments, demos of multiple use cases and a user study.

Bibliography

[1] A. AeroWand, 2016. http://www.accups.com/.

[2] S.-H. Baek, D. S. Jeon, X. Tong, and M. H. Kim. Simultaneous acquisition of polarimetric svbrdf and normals. *ACM Trans. Graph.*, 37(6):268:1–268:15, Dec. 2018.

[3] A. Borrego, J. Latorre, M. Alcaniz, and R. Llorens. Comparison of Oculus Rift and HTC Vive: Feasibility for Virtual Reality-Based Exploration, Navigation, Exergaming, and Rehabilitation. *Games for Health Journal*, 7(2):1–6, 2018.

[4] S. P. M. M. Controller, 2016. https://www.playstation.com/en-us/explore/accessories/playstation-move.

[5] G. Daydream, 2016. https://vr.google.com/daydream/.

[6] F. Durand. *3D Visibility : Analytical Study and Applications*. PhD thesis, Universite Grenoble I, 1999.

[7] N. I. Durlach and A. S. Mavor. *Virtual Reality: Scientific and Technological Challenges*. National Academies Press, 1995.

[8] Echolocus, 2014. http://www.echolocus.com/.

[9] R. P. Feynman, R. B. Leighton, and M. L. Sands. *The Feynman Lectures on Physics Volume I*. Addison-Wesley, 1963.

[10] H. V. Focus, 2018. https://www.vive.com/cn/product/vive-focus-en/.

[11] S. Gezici, Z. Tian, G. B. Giannakis, H. Kobayashi, A. F. Molisch, H. V. Poor, and Z. Sahinoglu. Localization via UltraWideband Radios. *IEEE Signal Processing Magazine*, 22(4):70–84, 2005.

[12] A. Ghosh, T. Chen, P. Peers, C. A. Wilson, and P. E. Debevec. Circularly polarized spherical illumination reflectometry. *ACM Trans. Graph.*, 29:162, 2010.

[13] B. Jung and M. Singh. Wireless Position Sensing using Magnetic Field of Two Transmitters, 2015. US 20150308861.

[14] A. Kadambi, V. Taamazyan, B. Shi, and R. Raskar. Polarized 3d: High-quality depth sensing with polarization cues. In *ICCV*, 2015.

[15] E. Labs, 2015. http://www.ellipticlabs.com/.

[16] P. Labs, 2015. https://www.pozyx.io/.

[17] H. Liu, H. Darabi, P. Banerjee, and J. Liu. Survey of Wireless Indoor Positioning Techniques and Systems. *IEEE Transactions on Systems, Man, and Cybernetics, Part C*, 37(6):1067–1080, 2007.

[18] C. Medina, J. C. Segura, and A. D. la Torre. Ultrasound Indoor Positioning System Based on a Low-Power Wireless Sensor Network Providing Sub-Centimeter Accuracy. *Sensors*, 13:3501–3526, 2013.

[19] L. M. Orion, 2016. https://www.leapmotion.com/product/vr.

[20] O. Quest, 2018. https://www.oculus.com/quest/features/.

[21] J. Riviere, I. Reshetouski, L. Filipi, and A. Ghosh. Polarization imaging reflectometry in the wild. *ACM Trans. Graph.*, 36(6):206:1–206:14, Nov. 2017.

[22] A. Rubin and J. P. Bellinghausen. Passive and Active Video Game Controllers with Magnetic Position Sensing, 2013. U.S. Patent 8,616,974.

[23] J. Shin, G. An, J.-S. Park, S. J. Baek, and K. Lee. Application of Precise Indoor Position Tracking to Immersive Virtual Reality with Translational Movement Support. *Multimed Tools Appl*, 75:12331–12350, 2016.

[24] S. S. System, 2016. `http://sixense.com/wireless`.

[25] A. E. F. Taylor. *Illumination Fundamentals*. Rensselaer Polytechnic Institute, 2000.

[26] F. Technologies, 2017. `https://www.youtube.com/watch?v=WgdksH0_laM`.

[27] O. V. Touch, 2016. `https://www3.oculus.com/en-us/touch/`.

[28] V. H. Vive, 2016. `https://www.htcvive.com/`.

[29] R. Wehner and M. Muller. The Significance of Direct Sunlight and Polarized Skylight in the Ant's Celestial System of Navigation. *PNAS*, 103(33):12575–12579, 2006.

[30] F. Weichert, D. Bachmann, B. Rudak, and D. Fisseler. Analysis of the Accuracy and Robustness of the Leap Motion Controller. *Sensors*, 13(5):6380–6393, 2013.

요약

본 논문에서는 POL360 이라고 불리우는 빛의 편광 원리를 활용한 3차원 위치 추적이 가능한 모바일 VR 기기용 컨트롤러를 제안하였다. POL360은 VR 헤드셋을 장착한 상황에서도 손의 움직임을 인지할 수 있도록 정확한 6 자유도의 위치 추적을 지원한다.

여타 VR 기기에서 활용하고 있는 기술에 비교하여 POL360은 세 가지의 장점을 보유하고 있다. (1) 모바일용 적합성 : PC 혹은 콘솔 기반의 VR 기기들은 6 자유도 위치 추적 기능을 지원하기 위하여 별도의 컴퓨팅 자원을 필요로 하거나 환경을 조성하기 위하여 별도의 설치 과정이 필요하다.

그에 비해, POL360은 오직 VR 헤드셋 밑에 작은 선편광 필름이 부착된 적외선 LED 모듈이 전부이므로 모바일용 적합성에서 우수함을 보여준다. (2) 온 디바이스 컴퓨팅(On-device computing) : POL360의 동작에 필요한 모든 연산은 기기 내의 작은 마이크로 프로세서에서 완료된다.

그러므로 VR 헤드셋과 동작 전체를 위한 추가적인 컴퓨팅 자원을 필요로 하지 않는다. (3) 위치 추적 고정확도 및 빠른 주사율 지원 : 훌륭한 모바일용 적합성에도 불구하고 POL360은 여타 기기에서 지원하는 위치 추적 정확도와 주사율 면에서 우수한 성능을 보인다.

위치 추적 정확도는 밀리미터 단위의 정확도를 보이며 업데이트 속도는 60Hz 이상 충분히 빠르므로 모바일 VR 경험을 해치지 않는다.

본 논문에서는 편광을 활용한 6 자유도 위치 추적에 수학적 접근을 최초로 증명하였고 현재 시장에 출시된 VR 헤드셋 시스템들과 직접적으로 호환되는 것을 보였다. POL360의 성능과 효용을 보여주기 위하여, 정량적 평가와 사용성 평가를 진행하였으며, 몇 가지의 게임 데모 까지 구현하였다.

주요어: 가상 현실, 6 자유도 위치 추적, 위치 추적, 공간 상호작용
학번: 2016-26445

Acknowledgements

First of all, I would like to express my sincere gratitude to Professor Gunhee Kim for his invaluable advise and guidance, from planning a better experiment to writing a good academic paper. His advice helped me in all the time of research and writing of this thesis.

I would also like to thank the collaborators, especially POLARIANT members who are Henry JEON, Jaden CHOI, Thomas CHOI, Ken LEE, Matthew LEE, Juno HONG, and Nikola PARK. I still think that this research might not have come to the world without their help.

I would like to express my sincere gratitude to the members of the SOCAR for supporting this study.

I also owe my thanks to my labmates in SNU Vision and Learning Laboratory.

Last but not the least, I would express a deep sense of gratitude to my parents and my sister for their constant love, encouragement, moral support and blessings throughout my entire life.